The analysis of piezomagnetoelastic energy harvesters under broadband random excitations

S. F. Ali,[1,a)] S. Adhikari,[1,b)] M. I. Friswell,[1] and S. Narayanan[2]
[1]*College of Engineering, Swansea University, Singleton Park, Swansea SA2 8PP, United Kingdom*
[2]*Indian Institute of Technology Madras, Chennai, India*

(Received 13 January 2011; accepted 29 January 2011; published online 6 April 2011)

This paper presents an analysis of piezomagnetoelastic energy harvesters under broadband random ambient excitations for the purpose of powering low-power electronic sensor systems. Their nonlinear behavior as a result of vibration in a magnetic field makes piezomagnetoelastic energy harvesters different from classical piezoelastic energy harvesters. An equivalent linearization-based analytical approach is developed for the analysis of harvested power. A closed-form approximate expression for the ensemble average of the harvested power is derived and validated against numerical Monte Carlo simulation results. Our results show that it is possible to optimally design the system such that the mean harvested power is maximized for a given strength of the input broadband random ambient excitation. © *2011 American Institute of Physics*. [doi:10.1063/1.3560523]

I. INTRODUCTION

The evolution of electronic devices since the beginning of micro and nanoelectronics has brought about exponential growth in computational power in ever-shrinking systems; the associated increase in functionality brings a revolution in systems targeting wearable healthcare, lifestyle, and industrial monitoring applications.

As systems continue to shrink, less energy is required onboard. This has allowed another energy paradigm, namely energy harvesting (also referred to as energy scavenging) from the environment. A decade of research in the field of energy harvesting has led to efficient capture of small amounts of energy from the environment and their transformation into electrical energy. Energy-autonomous systems using energy harvesting are particularly attractive when long-term remote deployment is needed or wherever a natural long-term energy source is available (such as temperature or vibrations) for continuous replenishment of energy consumed by the system. Such an inexhaustible energy supply is a significant advantage over a battery supply or mains power. Extended lifetime and autonomy are particularly advantageous in systems with limited accessibility, such as medical implants and infrastructure-integrated micro-sensors, wireless sensor nodes used for structural health monitoring, embedded and implanted sensor nodes for medical applications, recharging the batteries of large systems, monitoring tire pressure in automobiles, powering unmanned vehicles, and running household security systems.

As described by Williams and Yates,[1] the three basic vibration-to-electric energy conversion mechanisms are electromagnetic,[1–4] electrostatic,[5,6] and piezoelectric[7–10] transductions. In the last decade, these transduction mechanisms have been investigated by numerous researchers for vibration-based energy harvesting and extensive discussions can be found in existing review articles.[5,9,11,12]

Regardless of the transduction mechanism, a primary issue in vibration-based energy harvesting is that the best performance of a generator is usually limited to excitation at its fundamental resonance frequency. If the applied ambient vibration deviates slightly from the resonance condition then power output is drastically reduced. Hence, a major issue in energy harvesting is to enable broadband energy harvesters.[13,14] Thus, researchers have recently focused on the concept of broadband energy harvesting to solve this issue with different approaches.

The most recent addition to broadband energy harvesters is piezomagnetoelastic systems.[14] This magnetoelastic structure (described in the following section) was first investigated by Moon and Holmes[15] as a mechanical structure that exhibits strange attractor motions. Erturk *et al.*[14] investigated the potential of this device for energy harvesting when the excitation is harmonic and demonstrated an order of magnitude larger power output over the linear system (without magnets) for nonresonant excitation. Litak *et al.*[16] considered the performance of nonlinear piezomagnetoelastic system under random excitations using numerical methods.

The theoretical analysis of piezomagnetoelastic systems is absent in the literature. Analysis of a nonlinear piezomagnetoelastic energy harvesting system under random excitations requires solution of the multidimensional Fokker–Planck equation to obtain the governing probability density function of the harvested power. This paper considers a different approach and stochastically linearizes the system to develop an equivalent model of the overall system. The linear model is then analyzed to determine probability density functions of the system response and the power scavenged by the system. The paper is organized as follows: The next section describes the piezomagnetoelastic harvester. Details of the stochastic linearization technique are also given. A brief description of stochastic random vibration theory and the three nonlinear equations that must be solved to obtain the equivalent linear system are reported in Sec. III. The equivalent linear system under zero-mean white noise excitation is analyzed in Sec. IV. Numerical results are reported in Sec. V.

[a)]Electronic mail: sk.faruque.ali@gmail.com.
[b)]Electronic mail: s.adhikari@swansea.ac.uk.

II. PIEZOMAGNETOELASTIC ENERGY HARVESTERS

The device consists of a ferromagnetic cantilever beam that is excited at the support (see Fig. 1). Two permanent magnets are located symmetrically on the base near the free end. The distance between the beam and the magnets determines the stable equilibrium points. Here we are interested in the case when the system has three equilibrium positions, two of which are stable, and the mechanical system is characterized by the classical double-well potential. The nondimensional equations of motion for this system are

$$\ddot{x} + 2\zeta\dot{x} - \frac{1}{2}x(1-x^2) - \chi v = f(t), \tag{1}$$

$$\dot{v} + \lambda v + \kappa\dot{x} = 0, \tag{2}$$

where x is the dimensionless transverse displacement of the beam tip, v is the dimensionless voltage across the load resistor, χ is the dimensionless piezoelectric coupling term in the mechanical equation, κ is the dimensionless piezoelectric coupling term in the electrical equation, $\lambda \propto 1/R_l C_p$ is the reciprocal of the dimensionless time constant of the electrical circuit, R_l is the load resistance, and C_p is the capacitance of the piezoelectric material. The force $f(t)$ is proportional to the base acceleration on the device. A simulation-based nonlinear analysis for random base excitation is reported by the authors in Ref. 16. Gaussian white noise excitation, with zero mean and specified variance, was assumed for the simulations. The study demonstrated that the dynamics of the system is a double-well potential and the greatest energy generation occurs when the system moves between the potential wells.

Equation (1) is a nonlinear equation with nonlinearity in the stiffness term, whereas Eq. (2) is a linear equation. To facilitate the linearization process, Eq. (1) can be rewritten as

$$\ddot{x} + 2\zeta\dot{x} + g(x) - \chi v = f(t). \tag{3}$$

The nonlinear stiffness is represented as $g(x) = -\frac{1}{2}(x - x^3)$. This paper will develop a linearized model for the Duffing equation [Eq. (3)] based on the stochastic linearization approach.[17]

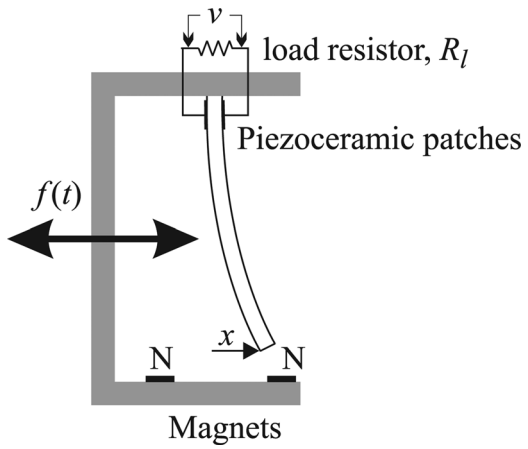

FIG. 1. Schematic diagram of magnetopiezoelastic device (Ref. 14). Reprinted with permission from Appl. Phys. Lett. **94**, 254102 (2009). Copyright 2009, American Institute of Physics.

Assuming a nonzero-mean random excitation [i.e., $f(t) = f_0(t) + m_f$] and a nonzero-mean system response [i.e., $x(t) = x_0(t) + m_x$], the following equivalent linear system is considered,

$$\ddot{x}_0 + 2\zeta\dot{x}_0 + a_0 x_0 + b_0 - \chi v = f_0(t) + m_f \tag{4}$$

where $f_0(t)$ and $x_0(t)$ are zero-mean random processes, m_f and m_x are the mean of the original processes $f(t)$ and $x(t)$ respectively, a_0 and b_0 are the constants to be determined, with $b_0 = m_f$ and a_0 the square of the natural frequency of the linearized system ω_{eq}^2. Stochastic moments of the nonlinear and the linearized model outputs will be matched by minimizing the expectation of the error norm, i.e., $(E[\varepsilon^2]$, with $\varepsilon = g(x) - a_0 x_0 - b_0)$. To determine the constants a_0 and b_0 in terms of the statistics of the response x, we take partial derivatives of the error norm with respect to a_0 and b_0 and equate them to zero individually.

$$\frac{\partial}{\partial a_0}E[\varepsilon^2] = E[g(x)x_0] - a_0 E[x_0^2] - b_0 E[x_0] \tag{5}$$

$$\frac{\partial}{\partial b_0}E[\varepsilon^2] = E[g(x)] - a_0 E[x_0] - b_0. \tag{6}$$

Equating Eqs. (5) and (6) to zero, we get,

$$\begin{aligned} a_0 &= \frac{E[g(x)x_0]}{E[x_0^2]} \\ &= \frac{E[g(x)x_0]}{\sigma_x^2} \end{aligned} \tag{7}$$

$$\begin{aligned} b_0 &= E[g(x)]. \\ &= m_f \end{aligned} \tag{8}$$

As a special case, if we assume that $x(t)$ is a Gaussian random process, the expressions in Eqs. (7) and (8) can be further simplified[17,18] as,

$$\begin{aligned} a_0 &= \mathrm{E}\left[\frac{d}{dx}g(x)\right] \\ &= -\frac{1}{2}\left(1 - 3E[x^2]\right) \\ &= -\frac{1}{2}\left\{1 - 3\sigma_x^2 - 3m_x^2\right\} \end{aligned} \tag{9}$$

which gives

$$3m_x^2 + 3\sigma_x^2 - 2a_0 - 1 = 0 \tag{10}$$

and

$$\begin{aligned} m_f &= E[g(x)] \\ &= -\frac{1}{2}\left(E[x] - E[x^3]\right). \end{aligned} \tag{11}$$

Note that for a nonzero-mean Gaussian process x with mean m_x and its zero-mean part x_0, we have the following relations.

$$E[x_0^3] = E[(x - m_x)^3] = E[x^3] - 3m_x\sigma_x^2 - m_x^3. \tag{12}$$

Since for a zero-mean Gaussian process $E[x_0^3] = 0$, using the relation in Eq. (12) we get,

$$E[x^3] = 3m_x\sigma_x^2 + m_x^3. \tag{13}$$

Substituting $E[x^3]$ from Eq. (13) into Eq. (11) we get

$$m_f = -\frac{1}{2}\left\{m_x - \left(3m_x\sigma_x^2 + m_x^3\right)\right\} \tag{14}$$

which gives

$$m_x\left(m_x^2 + 3\sigma_x^2 - 1\right) - 2m_f = 0 \tag{15}$$

where m_x and σ_x are the mean and standard deviation of the system response x.

The process of statistical linearization reduces to finding three unknowns a_0, m_x and σ_x with only two equations [Eqs. (10) and (15)]. Another expression for σ_x can be obtained from the linearized system equations.

Eq. (4) along with Eq. (2) can be rewritten as

$$\ddot{x}_0 + 2\zeta\dot{x}_0 + a_0x_0 - \chi\upsilon = f_0(t) \tag{16}$$

$$\dot{\upsilon} + \lambda\upsilon + \kappa\dot{x} = 0. \tag{17}$$

Taking the Fourier transform of Eqs. (16) and (17), we get

$$\begin{bmatrix} (a_0 - \Omega^2) + 2i\Omega\zeta & -\chi \\ i\Omega\kappa & (i\Omega + \lambda) \end{bmatrix} \begin{Bmatrix} X(\Omega) \\ V(\Omega) \end{Bmatrix} = \begin{Bmatrix} F_0(\Omega) \\ 0 \end{Bmatrix}. \tag{18}$$

Inverting the coefficient matrix, the displacement and voltage in the frequency domain can be obtained as

$$\begin{Bmatrix} X \\ V \end{Bmatrix} = \frac{1}{\Delta}\begin{bmatrix} (i\Omega + \lambda) & \chi \\ -i\Omega\kappa & (a_0 - \Omega^2) + 2i\Omega\zeta \end{bmatrix} \begin{Bmatrix} F_0 \\ 0 \end{Bmatrix} \tag{19}$$

$$= H(\Omega)\begin{Bmatrix} F_0 \\ 0 \end{Bmatrix} \tag{20}$$

where $H(\Omega)$ is the 2×2 matrix of frequency-response functions and the determinant of the coefficient matrix is

$$\Delta(i\Omega) = (i\Omega)^3 + (2\zeta + \lambda)(i\Omega)^2 + (2\zeta\lambda + \kappa\chi + a_0)(i\Omega) + \lambda a_0. \tag{21}$$

III. A BRIEF OVERVIEW OF STATIONARY RANDOM VIBRATION

We consider the excitation $f_0(t)$ to be a zero-mean, weakly stationary, Gaussian, broadband random process. To obtain statistics of random response quantities such as displacement of the mass $x(t)$ and the voltage $v(t)$, one needs to solve the coupled stochastic differential equations [Eqs. (16) and (17)]. However, analytical results developed within the theory of random vibration allow us to bypass numerical solutions because we are interested in the average values of the output random processes.

Since $f_0(t)$ is a weakly stationary random process, its autocorrelation function depends only on the difference in the time instants, and thus

$$\mathrm{E}[f_0(\tau_1)f_0(\tau_2)] = R_{f_0f_0}(\tau_1 - \tau_2). \tag{22}$$

This autocorrelation function can be expressed as the inverse Fourier transform of the spectral density $\Phi_{f_0f_0}(\Omega)$ as

$$R_{f_0f_0}(\tau_1 - \tau_2) = \int_{-\infty}^{\infty} \Phi_{f_0f_0}(\Omega)\exp[i\Omega(\tau_1 - \tau_2)]d\Omega. \tag{23}$$

For a damped linear system of the form shown in Eq. (20), it can be shown that[17,19] the spectral density of $X(\Omega)$ is related to the spectral density of the excitation F_0 by

$$\Phi_{x_0x_0}(\Omega) = |H_{11}(\Omega)|^2\Phi_{f_0f_0}(\Omega). \tag{24}$$

where $H_{11}(\Omega)$ is the element in the first row and column of the matrix $H(\Omega)$. In this paper we are interested in the standard deviation of the response, σ_x, given as

$$\sigma_x^2 = \sigma_{x0}^2 = \int_{-\infty}^{\infty} H_{11}(\Omega)^2\Phi_{f_0f_0}d\Omega \tag{25}$$

where $\Phi_{f_0f_0}$ is a constant for the weakly stationary, white noise process.

Combining Eqs. (19), (20), (21), and (25), we get

$$\sigma_x^2 = \Phi_{f_0f_0}\int_{-\infty}^{\infty} \frac{\lambda^2 + \Omega^2}{\Delta(\Omega)\Delta^*(\Omega)}d\Omega. \tag{26}$$

The calculation of the integral on the right-hand side of Eq. (26) in general requires the calculation of integrals of the following form

$$I_n = \int_{-\infty}^{\infty} \frac{\Xi_n(\Omega)\,d\Omega}{\Lambda_n(\Omega)\Lambda_n^*(\Omega)} \tag{27}$$

where the polynomials have the form

$$\Xi_n(\omega) = p_{n-1}\Omega^{2n-2} + p_{n-2}\Omega^{2n-4} + \cdots + p_0 \tag{28}$$

$$\Lambda_n(\omega) = q_n(i\Omega)^n + q_{n-1}(i\Omega)^{n-1} + \cdots + q_0. \tag{29}$$

Following Roberts and Spanos[17] and Adhikari *et al.*[20] this integral can be evaluated as

$$I_n = \frac{\pi}{q_n}\frac{\det[N_n]}{\det[D_n]}. \tag{30}$$

Here the $m \times m$ matrices are defined as

$$\mathrm{N}_n = \begin{bmatrix} p_{n-1} & p_{n-2} & & \cdots & & & p_0 \\ -q_n & q_{n-2} & -q_{n-4} & q_{n-6} & \cdots & 0 & \cdots \\ 0 & -q_{n-1} & q_{n-3} & -q_{n-5} & \cdots & 0 & \cdots \\ 0 & q_n & -q_{n-2} & q_{n-4} & \cdots & 0 & \cdots \\ 0 & \cdots & & & \cdots & 0 & \cdots \\ 0 & 0 & & & \cdots & -q_2 & q_0 \end{bmatrix} \tag{31}$$

and

$$\mathrm{D}_n = \begin{bmatrix} q_{n-1} & -q_{n-3} & q_{n-5} & -q_{n-7} & & & \\ -q_n & q_{n-2} & -q_{n-4} & q_{n-6} & \cdots & 0 & \cdots \\ 0 & -q_{n-1} & q_{n-3} & -q_{n-5} & \cdots & 0 & \cdots \\ 0 & q_n & -q_{n-2} & q_{n-4} & \cdots & 0 & \cdots \\ 0 & \cdots & & & \cdots & 0 & \cdots \\ 0 & 0 & & & \cdots & -q_2 & q_0 \end{bmatrix}. \tag{32}$$

Comparing Eqs. (21) and (26) with the general integral in Eqs. (27) and (28) we have

$$\begin{aligned} &n = 3, \\ &p_2 = 0, \quad p_1 = 1, \quad p_0 = \lambda^2, \text{ and} \\ &q_3 = 1, \quad q_2 = (2\zeta + \lambda), \quad q_1 = (2\lambda\zeta + \kappa\chi + a_0), \quad q_0 = a_0\lambda. \end{aligned} \tag{33}$$

Now using Eq. (33), the integral in Eq. (30) becomes,

$$I_n = \frac{\pi(a_0 + 2\lambda\zeta + \lambda^2)}{a_0\left(4\lambda\zeta^2 + 2\zeta\kappa\chi + 2\zeta a_0 + 2\lambda^2\zeta + \lambda\kappa\chi\right)}. \tag{34}$$

Combining Eq. (34) with Eq. (26) and then simplifying the resulting expression we obtain the final relation between a_0 and σ_x, which is given as

$$\begin{aligned} a_0\sigma_x^2\left(4\lambda\zeta^2 + 2\zeta\kappa\chi + 2\zeta a_0 + 2\lambda^2\zeta + \lambda\kappa\chi\right) \\ - \pi\Phi_{f_0f_0}\left(a_0 + 2\lambda\zeta + \lambda^2\right) = 0. \end{aligned} \tag{35}$$

Equation (35) along with Eqs. (10) and (15) provide three equations to solve for the unknown variables a_0, σ_x, and m_x. Analytical solutions of Eqs. (10), (15), and (35) are not possible and one should make use of numerical schemes. In the next section, solutions for zero-mean white noise excitation is shown. To summarize, one has to solve for m_x, σ_x, and a_0 from the following three nonlinear coupled equations,

$$\begin{aligned} 3m_x^2 + 3\sigma_x^2 - 2a_0 - 1 = 0 \\ m_x\left(m_x^2 + 3\sigma_x^2 - 1\right) - 2m_f = 0 \\ a_0\sigma_x^2\left(4\lambda\zeta^2 + 2\zeta\kappa\chi + 2\zeta a_0 + 2\lambda^2\zeta + \lambda\kappa\chi\right) \\ -\pi\Phi_{f_0f_0}\left(a_0 + 2\lambda\zeta + \lambda^2\right) = 0. \end{aligned} \tag{36}$$

IV. ZERO–MEAN WHITE NOISE EXCITATION

A. Determination of σ_x, a_0, and m_x

Without loss of generality the external excitation can be assumed to be a zero-mean white noise process, i.e., $m_f = 0$. This largely simplifies our analysis and provides a simple relation between the mean (m_x) and the standard deviation (σ_x) of the response. Putting $m_f = 0$ in Eq. (15) we get,

$$m_x\left(m_x^2 + 3\sigma_x^2 - 1\right) = 0 \tag{37}$$

which gives either $m_x = 0$ or $m_x = \sqrt{1 - 3\sigma_x^2}$.

Substituting $m_x = 0$ in Eq. (10) we get

$$3\sigma_x^2 = 1 + 2a_0. \tag{38}$$

Equation (38) shows that for $m_x = 0$ and for any real $a_0 \geq 0$, we have $\sigma_x^2 \geq \frac{1}{3}$.

Substituting $m_x = \sqrt{1 - 3\sigma_x^2}$ in Eq. (10) we get

$$\begin{aligned} 3(1 - 3\sigma_x^2) + 3\sigma_x^2 - 2a_0 - 1 = 0, \\ 1 - 3\sigma_x^2 - a_0 \qquad\qquad = 0 \end{aligned} \tag{39}$$

which gives

$$3\sigma_x^2 = 1 - a_0. \tag{40}$$

Equation (40) shows that for $m_x^2 = 1 - 3\sigma_x^2$ and real, positive a_0, we have $\sigma_x^2 \in [0, \frac{1}{3}]$.

This, on the other hand, bounds $a_0 \in [0, 1]$. A further analysis will show that $a_0 = m_x^2$.

Substituting Eq. (38) and Eq. (40) separately in Eq. (35) we obtain the following two cubic polynomial equations respectively.

$$\begin{aligned} &4\zeta a_0^3 + \left(8\lambda\zeta^2 + 4\lambda^2\zeta + 4\kappa\chi\zeta + 2\zeta + 2\lambda\kappa\chi\right)a_0^2 \\ &\quad + \left(4\lambda\zeta^2 + 2\lambda^2\zeta + 2\kappa\chi\zeta + \lambda\kappa\chi - 3\Phi_{f_0f_0}\pi\right)a_0 \\ &\quad - 3\Phi_{f_0f_0}\pi\lambda(\lambda + 2\zeta) = 0 \end{aligned} \tag{41}$$

$$\begin{aligned} &2\zeta a_0^3 + \left(4\lambda\zeta^2 + 2\lambda^2\zeta + 2\kappa\chi\zeta - 2\zeta + \lambda\kappa\chi\right)a_0^2 \\ &\quad - \left(4\lambda\zeta^2 + 2\lambda^2\zeta + 2\kappa\chi\zeta + \lambda\kappa\chi - 3\Phi_{f_0f_0}\pi\right)a_0 \\ &\quad + 3\Phi_{f_0f_0}\pi\lambda(\lambda + 2\zeta) = 0. \end{aligned} \tag{42}$$

Numerical solutions show that Eq. (41) has a single real positive root and Eq. (42) has two real positive roots for any given value of $\Phi_{f_0f_0}$.

B. Determination of $E[v^2]$

The spectral density of the voltage generated across the harvester can be related to the excitation as

$$\Phi_{vv}(\Omega) = \left|H_{21}(\Omega)^2\right|\Phi_{f_0f_0}(\Omega), \tag{43}$$

where $H_{21}(\Omega)$ is the element in the second row and first column of the matrix $H(\Omega)$ [see Equation (19)].

$$E[v^2] = \int_{-\infty}^{\infty} \left|H_{21}(\Omega)^2\right|\Phi_{f_0f_0}d\Omega \tag{44}$$

where $\Phi_{f_0f_0}$ is a constant for a weakly stationary, white noise process.

Combining Eqs. (19), (20), (21), and (44), we get

$$E[v^2] = \Phi_{f_0f_0}\int_{-\infty}^{\infty} \frac{\kappa^2\Omega^2}{\Delta(\Omega)\Delta^*(\Omega)}d\Omega. \tag{45}$$

Proceeding in a similar way to Sec. III we find an expression for $E[v^2]$ as

$$E[v^2] = \frac{\kappa^2\lambda a_0}{a_0\left(4\lambda\zeta^2 + 2\zeta\kappa\chi + 2\zeta a_0 + 2\lambda^2\zeta + \lambda\kappa\chi\right)}\pi\Phi_{f_0f_0}. \tag{46}$$

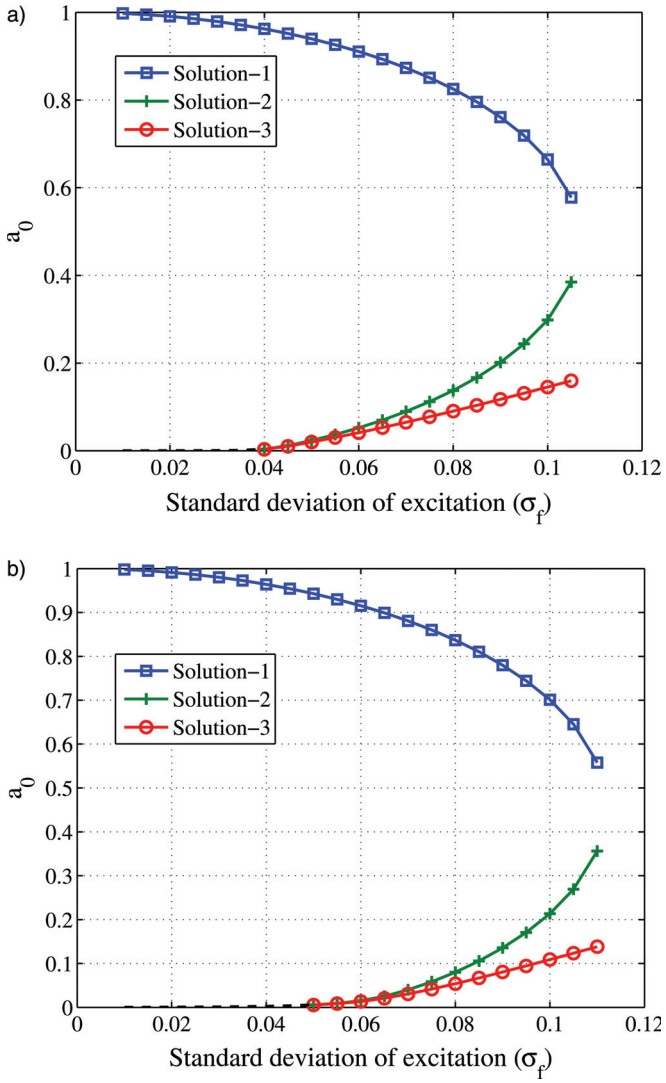

FIG. 2. (Color online) Square of the natural frequency of the equivalent linear system for different standard deviations of the excitation (σ_f) for (a) $\lambda = 0.01$ and (b) $\lambda = 0.05$. The black dashed line represents unstable solution at $a_0 = 0$.

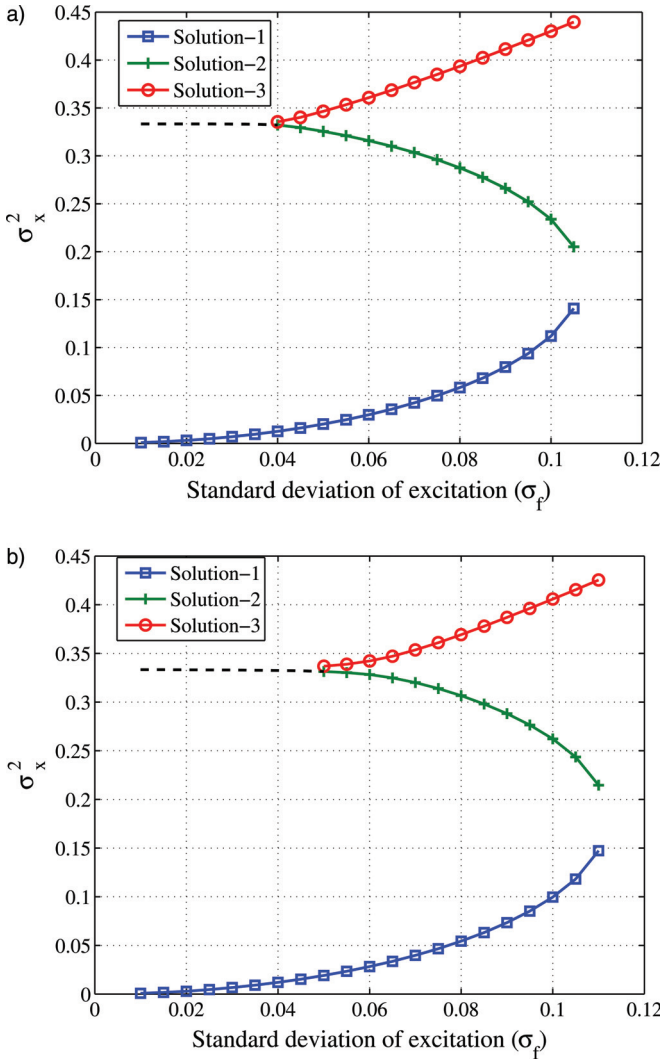

FIG. 3. (Color online) Square of standard deviation of the response under different standard deviations of the excitation for (a) $\lambda = 0.01$ and (b) $\lambda = 0.05$. The black dashed line represents unstable solution at $a_0 = 0$.

V. NUMERICAL ANALYSIS

As discussed in Sec. IV A, analytical solutions of Eqs. (41) and (42) are not feasible. Numerical methods are used to solve for different values of σ_x, a_0, and m_x. The solutions of Eqs. (41) and (42) for various values of standard deviation of the excitation are reported.

The system parameters have been taken as follows:[14] $\zeta = 0.01$, $\chi = 0.05$, and $\kappa = 0.5$, while λ varied between 0.01 and 0.05. The excitation $f(t)$ is considered stationary Gaussian white noise with standard deviation σ_f ranging from 1% to 11%. Higher values of standard deviation are not considered, as statistical linearization would fail to represent the system for higher standard deviations.

The nonlinear piezomagnetoelastic system given by Eq. (1) represents a Duffing-type equation of motion. The nonlinear system has three equilibrium points, two stable equilibrium points at $x = \pm 1$ and one unstable equilibrium point at the origin ($x = 0$). Numerical simulations show that Eq. (41) has a single real positive solution for a_0, whereas Eq. (42) has two real positive solutions. The solutions for different standard deviations of excitation are shown in Fig. 2. Solution-1 and Solution-2 are the solutions for Eq. (42), i.e., where $m_x = \sqrt{1 - 3\sigma_x^2}$, and Solution-3 is obtained by solving Eq. (41), i.e., the solution representing the zero-mean response. This representation of the solutions is the same for all figures reported in this article.

Figures 2(a) and 2(b) are for $\lambda = 0.01$ and $\lambda = 0.05$, respectively. Note that a_0 is the square of the natural frequency of the equivalent linear system [see Equation (4)] and therefore cannot be negative. The blue curve (with square markers) represents both of the $x = \pm 1$ stable equilibrium points. The black dotted line represents the solution $a_0 = 0$ up to $\sigma_f = 0.04$ and $\sigma_f = 0.05$ for $\lambda = 0.01$ and $\lambda = 0.05$ respectively. This solution is the unstable equilibrium point of the system. Therefore the only practical solution for the system below $\sigma_f = 0.04$ for electrical constant $\lambda = 0.01$ and below $\sigma_f = 0.05$ for $\lambda = 0.05$ is given by the blue curve with square markers. At this stage the system remains in one of the potential wells represented by $x = \pm 1$.

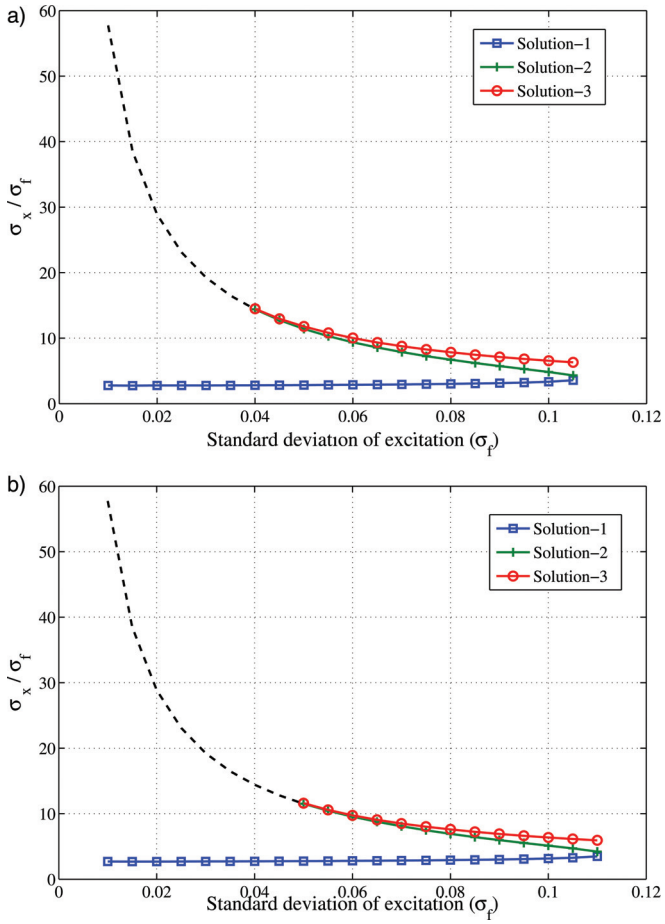

FIG. 4. (Color online) Ratio of standard deviation of displacement to standard deviation of the excitation under different standard deviations of the excitation for (a) $\lambda = 0.01$ and (b) $\lambda = 0.05$. The black dashed line represents the unstable solution at $a_0 = 0$.

When the excitation standard deviation reaches the cut off ($\sigma_f = 0.04$ for $\lambda = 0.01$ and $\sigma_f = 0.05$ for $\lambda = 0.05$) the system has enough energy to cross the potential barrier and could jump to the other potential well. This jump from one potential well to another generates more energy, as will be shown later. These cut-off standard deviations of the excitation are explained as stochastic resonance phenomena in Litak *et al.*[16]

Figure 3 shows the square of the standard deviation of the response versus the standard deviation of the excitation. It can be observed (and has been described in Sec. IV A) that two real positive solutions of σ_x^2 exist for $m_x \neq 0$. which have values less than $\frac{1}{3}$. Another real positive solution is obtained by solving Eq. (41), which results in $\sigma_x \geq \frac{1}{3}$.

Note that the square of the standard deviation of the response $\sigma_x^2 = \frac{1}{3}$ for Solution-2 and Solution-3, as long as the standard deviation of excitation $\sigma_f \leq 0.04$ and $\sigma_f \leq 0.05$ for $\lambda = 0.04$ and $\lambda = 0.05$, respectively. At the cut-off standard deviation of excitation the standard deviation of response could jump from Solution-1 to Solution-2 or Solution-3 (depending on the initial condition of the system), generating more power. This phenomenon is observed in the solution of the nonlinear system as shown in Litak *et al.*[16] Another point to note is that the σ_x^2 curves are similar for both $\lambda = 0.04$ and $\lambda = 0.05$, the only distinction being the cut-off value of σ_f. This shows that the electrical constant (λ) plays little role in the response of the system and that the mechanical and electrical systems are only weakly coupled.

Figure 4 shows the ratio of standard deviations of the response and the excitation. An order of magnitude increase in the standard deviation of the response is seen near the cut-off region. Figure 5 shows the variation of the square of the mean of the system responses for different values of σ_f. As described earlier, the third solution is the zero-mean response. Interestingly the mean responses seem to be converging to a particular value with increase in standard deviation of excitation. As the excitation noise is increased the oscillation of the magnetoelastic rod crosses the potential barrier between individual equilibria and keeps oscillating. Therefore the equivalent linearization does not represent any equilibrium value at higher excitation deviations, rather it shows a new point over which the system keeps oscillating.

The variance of voltage, which is a measure of the mean power harvested, is shown in Fig. 6 for $\lambda = 0.01$ and $\lambda = 0.05$. Figures 6(a) and 6(b) show that the voltage increases across the circuit near the cut-off values of the

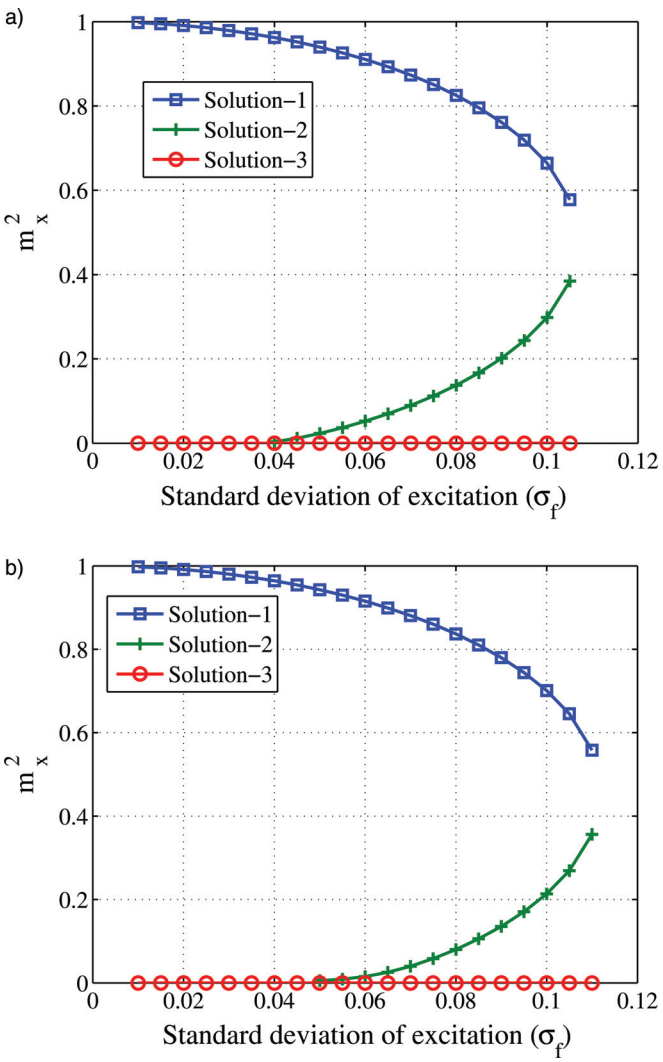

FIG. 5. (Color online) Square of the mean of the displacement response against the excitation standard deviation for (a) $\lambda = 0.01$ and (b) $\lambda = 0.05$.

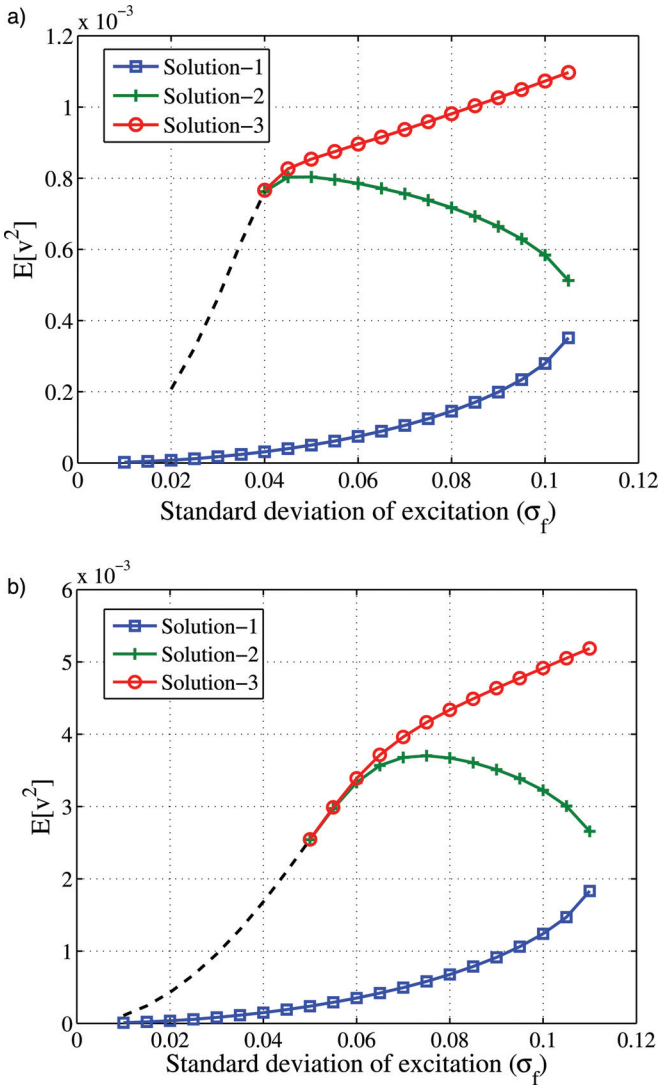

FIG. 6. (Color online) Variance of voltage against the excitation standard deviation for (a) $\lambda = 0.01$ and (b) $\lambda = 0.05$. The black dashed line represents unstable solution at $a_0 = 0$.

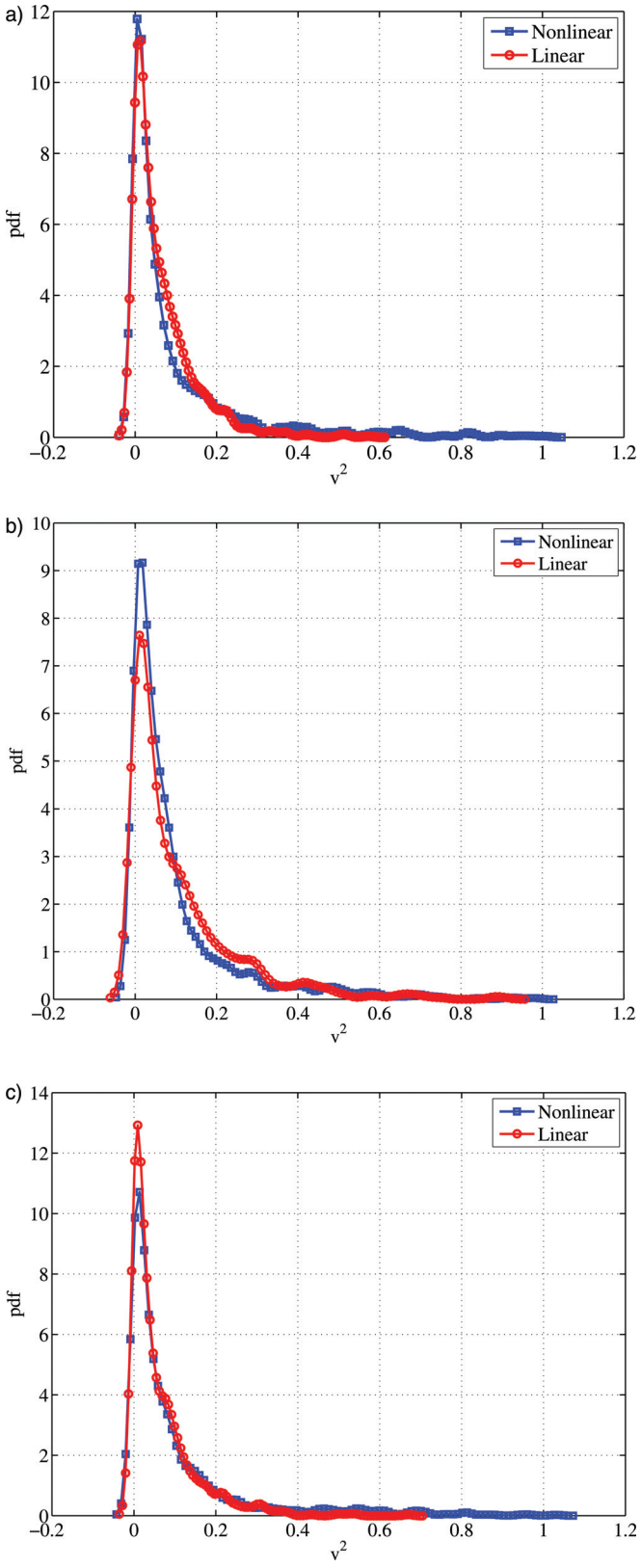

FIG. 7. (Color online) Probability density functions of the square of the voltage, i.e., mean power across the piezoelectric patch, v^2, for $\sigma_f = 0.1$ and $\lambda = 0.01$. (a) Solution-1, (b) Solution-2, (c) Solution-3.

excitation standard deviation. Note that the power remains very low for noise intensities below the cut-off value. The electrical constant λ significantly affects the voltage produced and, hence, the power generated. Note that this increase in power above the cut-off point is a result of changes in the electrical system, since the mechanical responses shown in Figs. 2–5 are almost identical. The practical implementation of a increase in λ requires a reduction in either electrical resistance or capacitance. This matches the reality, i.e, power increases with a decrease in resistance across the circuit. These requirements should be included in trade-off studies required for the design of a real system.

To validate our equivalent linear model simulation, results from the linear model are compared to that of the nonlinear system.[16] Simulations for both models were performed 5000 times and then the statistical responses were compared for different values of the linearized natural frequency at a particular excitation standard deviation. Figure 7 shows the probability density functions of the linear and nonlinear models for the excitation standard deviation $\sigma_f = 0.10$ and $\lambda = 0.01$. The results do not match exactly, but their closeness confirms that the equivalent linearization captured the significant dynamics of the nonlinear piezomagnetoelastic harvesters.

VI. CONCLUSION

Piezomagnetoelectric harvesters are best suited for broadband energy harvesting. These devices are nonlinear and their mechanical counterpart is represented by a Duffing-type oscillator. The device is nonlinear and can have chaotic motion, depending on the input excitation. Chaotic motion generates an order of magnitude larger power output over the linear system (without magnets) for nonresonant excitation. This paper develops an equivalent linear model of the nonlinear system. An analytical expression for the equivalent linear system is given. The following points are obtained from the analyses of the equivalent linear system:

- There exists a cut-off standard deviation of the input excitation, below which the power scavenged by the device is very low. The power generated by the device increases rapidly as the standard deviation of the input excitation is increased.
- This cut-off standard deviation of the input excitation changes with the electrical constant of the system. The lower the electrical constant (i.e., higher λ), the higher the cut-off standard deviation.
- The effect of variation in the electrical constant on the mechanical response of the system is relatively small. The mean and standard deviation of the system displacements are affected by the change in λ only near the cut-off standard deviation.
- The power generating capacity of the system increases with increasing λ. Thus, decreasing the resistance or capacitance of the system will increase the harvested power.

This article verifies the equivalent linear system with results obtained from simulation studies of the nonlinear system. To have a complete picture of the system behavior under random excitation one has to solve the Fokker–Planck equation. This remains for future study.

ACKNOWLEDGMENTS

Dr. S. F. Ali gratefully acknowledges the support of the Royal Society through a Newton International Fellowship.

[1]C. Williams and R. Yates, Sens. Actuators, A **52**, 8 (1996).
[2]D. P. Arnold, IEEE Trans. Magn. **43**, 3940 (2007).
[3]S. P. Beeby, R. N. Torah, M. J. Tudor, P. Glynne-Jones, T. O'Donnell, C. R. Saha, and S. Roy, J. Micromech. Microeng. **17**, 1257 (2007).
[4]R. Amirtharajah and A. Chandrakasan, IEEE J. Solid-State Circuits **33**, 687 (1998).
[5]S. P. Beeby, M. J. Tudor, and N. M. White, Meas. Sci. Technol. **17**, 175 (2006).
[6]E. Halvorsen, J. Microelectromech. Syst. **17**, 1061 (2008).
[7]H. A. Sodano, D. J. Inman and G. Park, The Shock and Vibration Digest. **36**, 197 (2004).
[8]N. E. Dutoit, B. L. Wardle, and S.-Gook Kim, Integrated Ferroelectrics. **71**, 121 (2005).
[9]S. Priya, J. Electroceramics **19**, 167 (2007).
[10]S. Ali, S. Adhikari, and M. I. Friswell, Smart Mater. Struct. **19**, 105010 (2010).
[11]H. A. Sodano, G. Park, and D. J. Inman, Strain **40**, 49 (2004).
[12]S. R. Anton and H. A. Sodano, Smart Mater. Struct. **16**, R1 (2007).
[13]B. Marinkovic and H. Koser, Appl. Phys. Lett. **94**, 103505 (2009).
[14]A. Erturk, J. Hoffmann, and D. J. Inman, Appl. Phys. Lett. **94**, 254102 (2009).
[15]F. C. Moon and P. J. Holmes, J. Sound Vib. **65**, 275 (1979).
[16]G. Litak, M. I. Friswell, and S. Adhikari, Appl. Phys. Lett. **96**, 214103 (2010).
[17]J. B. Roberts and P. D. Spanos, *Random Vibration and Statistical Linearization* (Dover Publications, Mineola, N. Y., 2003).
[18]I. E. Kazakov, Autom. and Remote Control (Engl. Transl.) **26**, 1201 (1965).
[19]N. C. Nigam, *Introduction to Random Vibration* (The MIT Press, Cambridge, Massachusetts, 1983).
[20]S. Adhikari, M. I. Friswell, and D. J. Inman, Smart Mater. Struct. **18**, 115005 (2009).